Magnetic Resonance in Medicine 45:486–494 (2001)

Automatic Scan Prescription for Brain MRI

Laurent Itti,* Linda Chang, and Thomas Ernst

Diagnostic brain MRI scans are usually performed by trained medical technologists who manually prescribe the position and orientation of a scanning volume. In this study, a fully automatic computer algorithm is described which compensates for variable patient positioning and acquires brain MRI scans in a predefined reference orientation. The method involves acquiring a rapid water-only pilot scan, segmenting the brain surface, and matching it to a reference surface. The inverse matching transformation is then used to adapt a geometric description of the desired scanning volume, defined relative to the reference surface, to the current patient. Both pilot scan and processing are performed within 30 sec. The method was tested in 25 subjects, and consistently recovered orientation differences between the reference and each subject to within ±5°. Compared to manual prescription, automatic scan prescription promises many potential benefits, including reduced scan times, reproducible scan orientations along anatomically preferable orientations, and better reproducibility for longitudinal studies. Magn Reson Med 45: 486–494, 2001. © 2001 Wiley-Liss, Inc.

Key words: MRI; registration; image processing; brain; scan acquisition; automatic

MRI scans are generally performed according to manual prescriptions by specially trained MR technologists. For instance, the determination of the location, size, and orientation of a scanning volume requires detailed input and adjustments by a technologist. A typical scanning session begins with the acquisition of a localizer or pilot scan, which provides an overview of the major anatomical features of a patient's organ to be scanned. The technologists then use the pilot scan to visually determine the location and orientation of scan planes for the subsequent series of high-resolution scans. However, manual prescription of scan geometry is relatively time consuming; for example, precise manual definition of scan orientation and boundaries can take up to several minutes when patients have unusual positions in the scanner. Therefore, operators often do not fully explore all degrees of freedom, such as 3D rotations, despite the relatively imprecise positioning of subjects in the scanner. Finally, manual scan prescription often is not reproducible as it suffers from both intra- and inter-operator variability—for instance, in defining the extent of anatomical coverage or the slice orientations. Consequently, MRI scans are typically performed in a non-standardized fashion, yielding scan orientations that vary from one patient to another. Therefore, there is a need for computer algorithms for the automatic prescription of MRI scans according to standardized protocols which could permit faster and more reproducible scans of the same organ at different points in time.

Harbor UCLA Research and Education Institute, Torrance, California.

*Correspondence to: Laurent Itti, University of Southern California, Hedco Neuroscience Building, HNB-30A, Los Angeles, CA 90089-2520. E-mail: itti@java.usc.edu

Received 15 May 2000; revised 8 August 2000; accepted 3 October 2000.

In this work we present a software algorithm for the automatic prescription of MRI scans of the human brain. The method is related to existing algorithms for post hoc image coregistration and reorientation. Such algorithms have been widely used in research to determine the difference in orientation and position between scans acquired on one or several different machines. Typically, the orientation and position of one scan are iteratively adjusted until they match those of another scan (1). The matching criterion can be based on a measure of generalized distance between 3D surface outlines of the brain from both scans (2,3), on distances between external or anatomical landmarks (4,5), or on comparison of image intensities in overlapping brain regions (6,7). Rather than reorienting scans after data acquisition to match a common reference template, our method directs the scanner to acquire scans that natively match the geometry (i.e., scanning volume boundaries and 3D orientation) of the reference template. The algorithm automatically determines an optimal scanning geometry, defined relative to a template human brain, that matches the positioning and morphology of a patient. For every new patient a pilot scan is first acquired, from which the outer surface of the patient's brain is automatically extracted. By automatically matching the patient's brain surface to the template brain surface using coregistration, geometric information about the size, location, and orientation of the current brain relative to the template brain is computed. The resulting transformation between current and template brains is finally used to transform the location and orientation of optimal scanning planes, as defined in the template, to the current patient. Subsequent scans can then be acquired according to the desired scanning geometry and independently of patient positioning (Fig. 1).

METHODS

MRI Scans

All MRI scans were acquired on a 1.5 T whole body scanner (GE Signa 5.8, Milwaukee, WI) equipped with fast shielded gradients (SR 120). The method was developed and tested using scans from 13 volunteers (training data sets), and subsequently validated with no further modification of the algorithm on scans from 12 additional volunteers (test data sets). These 25 scans constitute all the scans acquired for the purpose of this study, and no scans were excluded from the analysis. First, a single-shot fast spin echo scan with fat suppression was acquired (TE 900 msec, 5 mm slices with 1 mm gap, 256 × 256 matrix, and 25 slices), which essentially shows signal from CSF only due to its extremely long TE. Although such a scan contains little anatomical information for human interpretation (Fig. 1), it can be acquired in a very short time (typically 10–20 sec) and provides sufficient information for an automated segmentation of the cortical surface.

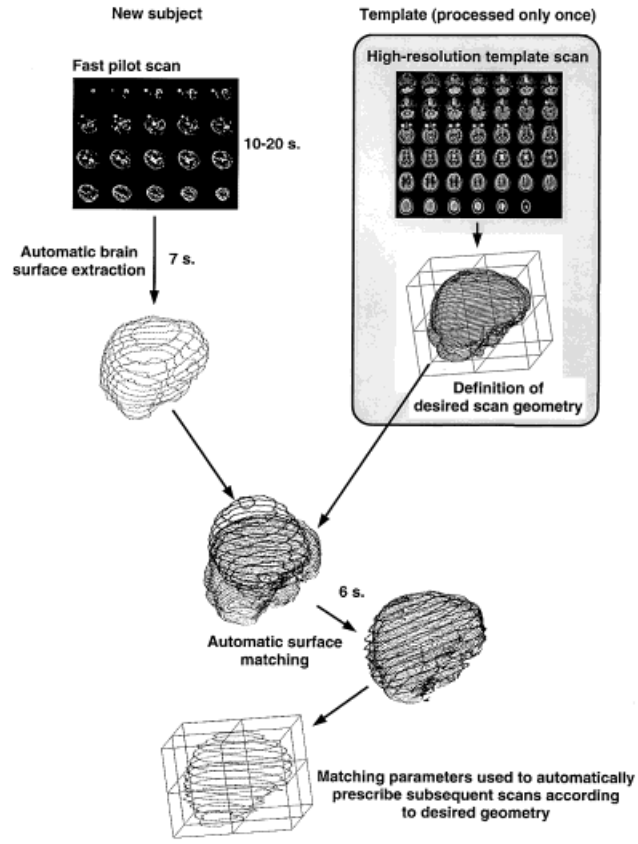

FIG. 1. Flow chart of the computer software algorithm utilized for automatic prescription of scan geometry. A reference template is created from a high-resolution MRI scan, and contains a brain surface and desired scanning geometry relative to that surface (top right). For each new subject (top left), a CSF pilot scan is acquired. The outer surface of the subject's brain is automatically segmented and matched to the reference surface. The 3D rotation resulting from matching the two surfaces is then used to transform the geometric description of the desired scanning volume from the reference to the current scan. Subsequent scans can finally be acquired according to this geometry, and will natively have a 3D orientation which matches that of the reference.

In three of the volunteers, the head was intentionally positioned in an extremely tilted position (see Fig. 2). Following off-line determination of the desired scan orientations, as described below, an additional validation scan was acquired according to the computed geometry. The validation scans used a segmented spin-echo echo planar imaging (EPI) sequence (TE 100 msec, TR 3000 msec, 5 mm slice with 1 mm gap, and 256 × 256 matrix).

Template

For the present study, a template was created containing a 3D geometric description of the outer surface of a human brain and a desired parallelepipedic scanning volume. The template brain surface was automatically segmented (3) from a high-resolution inversion-recovery scan of a normal volunteer (TR 4000 msec, TI 120 msec, TE 32 msec, 3.5 mm slices with no gap, and 256 × 256 matrix). The desired scanning geometry was defined relative to the template brain surface by manually selecting the 3D position, orientation, and size of a parallelepiped representing the volume to be scanned.

Image Processing

The algorithm to determine the spatial relationship between the brain in the current study and the template brain, and ultimately the slice plane orientations, was implemented as an extension of a customized coregistration software package developed in our laboratory (3,8,9). Typical processing times discussed in this study were obtained on a 500 MHz Compaq Alpha XP1000 Unix workstation. All algorithms described were written in language C.

The coregistration program is based on a two-step surface-matching algorithm. In the first primary step, the brain surface from the current CSF pilot scan is automatically extracted using an extension of the techniques described by Alpert et al. (10) and Mangin et al. (11). All processing is performed on a data set that is downsized by a factor of 2 in all three directions to reduce image processing time; hence, future pilot scans could be acquired at a lower resolution. Pixels with signal intensity outside the range of CSF intensity (e.g., background noise) are excluded using window thresholding: A pixel is considered CSF if its intensity is between 10% and 100% of the maximum intensity in the entire volume. The low threshold of 10% is chosen to include as much CSF as possible while excluding background noise. To avoid inclusion of the eyes in the brain segmentation, the eyes are eliminated using a 3D filter which maximally responds to a spherical object of 12-mm diameter on an empty background. The 3D convolution kernel for this filter hence contains values 1 inside the sphere and –1 outside. A threshold is applied to the result of the convolution to isolate the eyes, which are subsequently masked from the CSF scan. The resulting binary 3D volume within the accepted intensity range and with eyes removed is then subjected to isotropic 3D binary morphological dilation, with the objective of filling gaps in the outline of the brain derived from the CSF images. The morphological dilation operator replaces each non-zero pixel in the volume by a filled sphere of 3-cm diameter. Fast isotropic 3D dilation is obtained by thresholding an anisotropic chamfer distance map (3,12). Next, the dilated binary brain is isolated using an 8-connected 3D flooding algorithm, starting at the centroid of the dilated volume. As a result, non-brain structures with pixel intensities within the CSF range are eliminated. To recover the original brain size from the dilated and isolated binary brain, a 3D binary morphological erosion then is applied by thresholding an anisotropic chamfer distance map. Total processing time for this fully automatic brain segmentation is 7 sec.

In the second primary step, the brain surface from the current CSF scan is iteratively matched to that from the template. The surface from the current scan is considered mobile, whereas the template surface is a fixed reference. Therefore, 3D vertices are used to describe the current

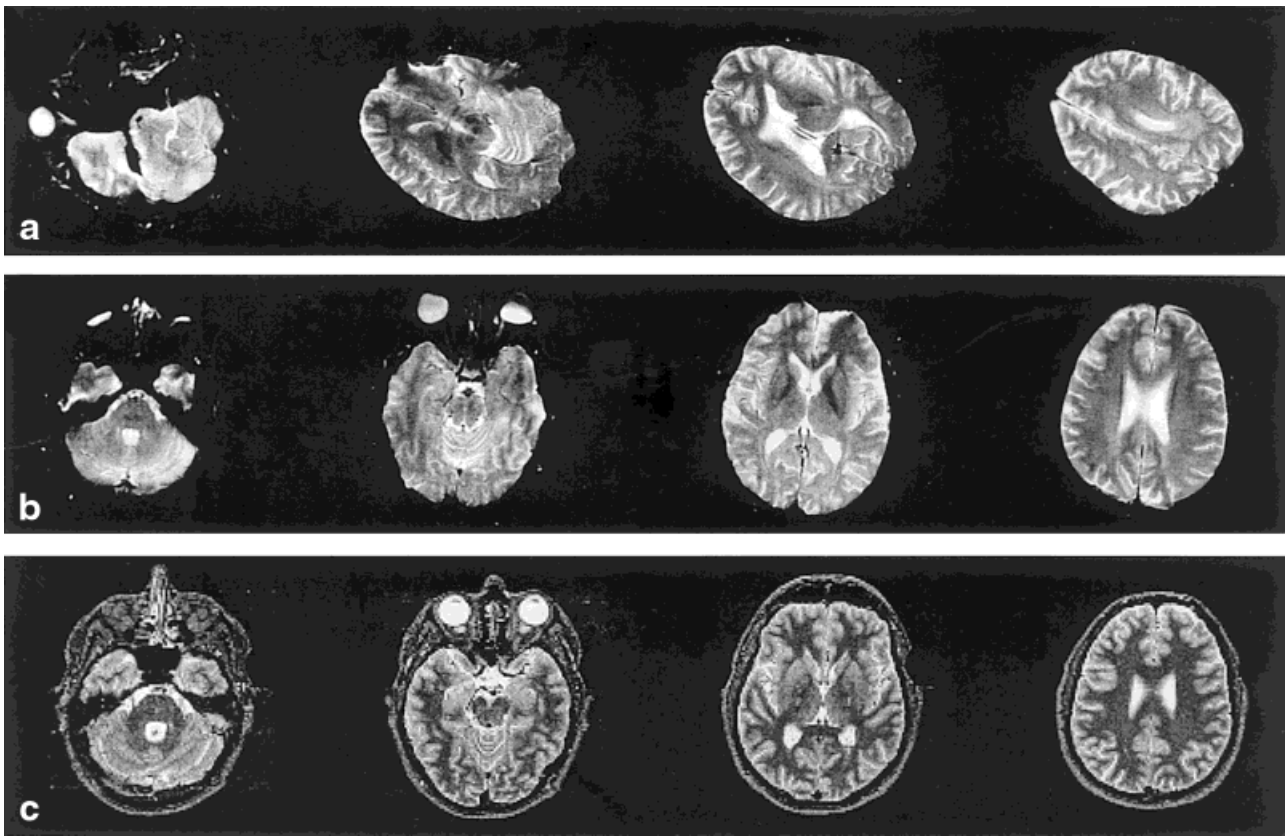

FIG. 2. MRI scans from a subject with markedly tilted head position, before (**a**) and after (**b**) adjusting the scan geometry. Note that the optimized scan (**a**) mirrors the slight rotation about the z-axis present in the reference template scan (**c**).

surface, whereas the template surface is represented by means of a chamfer distance map. Such a 3D distance map contains, for each pixel in a 3D volume, an approximation to the Euclidean distance between that particular pixel and the closest pixel on the template brain surface (3,13) (Fig. 3). Such a representation allows for fast computation of the distance between an arbitrary 3D vertex v and the closest point on the template brain surface, through a simple readout of the value in the distance map at the location of v (using trilinear interpolation). The computation of the distance map only needs to be performed once when the template is created, since it is associated with the template brain surface. To match the two brain surfaces, the vertices v of the mobile surface of the current patient, described by their 3D coordinates, are iteratively transformed to new vertices v′ using a 3D transformation with nine parameters:

$$v' = Av + T, \qquad [1]$$

where the vector T represents a translation (three parameters), and the 3×3 matrix A has six free parameters: three for rotations and three for scaling. The centers of mass of the two data sets are used to obtain an appropriate starting translation value for the iterative algorithm; the starting values for the rotations are 0 and those for scaling are 1. The mismatch between the two brain surfaces is then evaluated by calculating a generalized distance measure D from the locations of the transformed vertices v′ in the chamfer map. The distance measure is an approximation to the mean squared Euclidean distance between the vertices on the mobile surface and the reference surface. Thus, the generalized distance D provides a measure of the quality of fit between the two brain surfaces. Because the current CSF pilot scan may not cover the entire brain, the generalized distance measure D is defined in such a way that it is possible to match scans with incomplete overlap (3). Since the resulting distance measure may not be a continuous variable, Powell's minimization algorithm for nonregular functions is used to iteratively modify A and T in order to minimize the distance D between the two brain surfaces (14).

This initial surface matching is further refined using an alternate distance map; the convergence point of the initial matching is used as a starting point. The alternate distance map is identical to the original distance map except that it contains voids in the nasal sinus region (Fig. 3); consequently, the second surface matching step is insensitive to the inclusion of the sinuses in the mobile brain surface. This is necessary because large amounts of fluid in the nasal sinuses of a few subjects, due to sinusitis, were included in the initial brain segmentation. A similar strategy could be used to render the matching process insen-

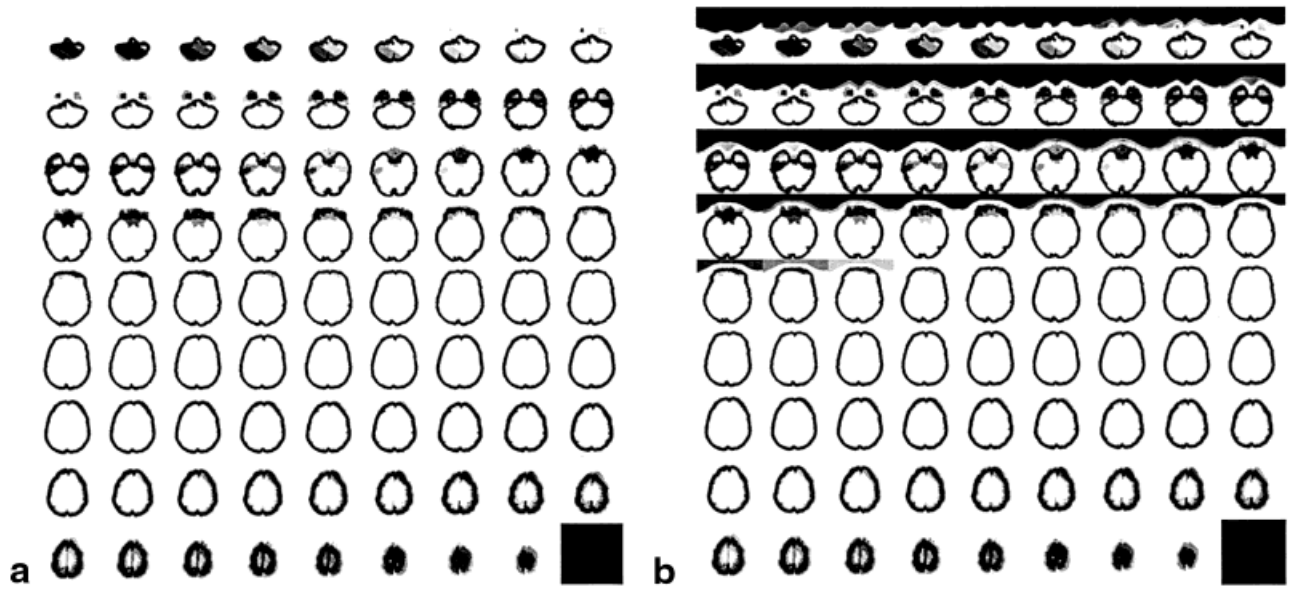

FIG. 3. Anisotropic chamfer distance map associated with the reference template brain (**a**). For each location the intensity in the map represents an approximation to the Euclidean distance between that location and the nearest location on the reference brain surface. In a refined version of the distance map (**b**) we have manually set the distance to zero (black) in the region of the nasal sinuses; vertices from the mobile surface falling in this region will thus be ignored during the computation of the generalized surface matching measure D. This modification renders the surface matching algorithm insensitive to segmentation artifacts in the region of the nasal sinuses. Similar modifications of the distance map could be used to render the algorithm robust to other classes of common structural abnormalities.

sitive to other segmentation artifacts. The total processing time for both surface matching steps is less than 6 sec.

Once the geometric relationship between template and current brain surface is known, it can be used to compute the boundaries and orientations of the desired scanning volume for the current patient. The geometric description of the desired scanning volume associated with the template brain (e.g., rotation of the slice planes relative to the brain) is simply converted to the frame of reference of the current brain, using the inverse of the best-fit transformation (see Eq. [1]). The desired scan geometry relative to the current brain can then be used to acquire all subsequent scans for the current patient.

Validation

The accuracy with which our algorithm was able to determine 3D rotations between the template and current brains was evaluated by comparing the positions of anatomical landmarks in the template scan and in the pilot CSF scan resliced according to the geometric transformation from the surface matching. Ideally, these anatomical landmarks should be at the same spatial locations in the template and resliced pilot scans, and all three rotation angles derived from comparing these landmarks should be close to zero. To determine the residual differences in the x-rotation between template and current scan (rotation about an axis along the left/right direction), a line joining the most inferior point of the frontal lobe and the most superior point of the cerebellum was manually drawn on the mid-sagittal slice. The angular difference between the line drawn on the template and on the current scan was then computed. To determine the y-rotation (rotation about an axis along the anterior/posterior direction), a line joining the centroids of both eyes was determined using the eye detection algorithm described above. Finally, to determine the z-rotation (rotation about an axis along the superior/inferior direction), a line was manually drawn along the midline, on the first transaxial slice above the ventricles. In this study, we detail estimated and residual rotation parameters, which are critical in evaluating the usefulness of the method, and simply report a summary of translation and scaling parameters.

RESULTS

The algorithm to extract the brain surfaces from the current pilot scan, as well as the surface matching, worked reliably in all 25 volunteers. Although the algorithm had been tuned and optimized using the first 13 subjects (the training set), it was successfully applied with no further modification to the 12 additional volunteers who were scanned subsequently (the test set). Using separate training and test sets allowed us to determine whether our optimizations of the algorithm to yield good performance on the training set would generalize to entirely new scans after algorithmic development had been frozen. Typical processing time for the entire automatic scan prescription, including pilot scan, brain surface extraction, surface matching, and computation of desired scanning geometry, was approximately 30 sec (with processing done on a 500 MHz Compaq Alpha XP1000 Unix workstation; see Methods). Figures 4 and 5 show the individual angular differences between patients and template, as estimated from the automatic prescription, for the training and test

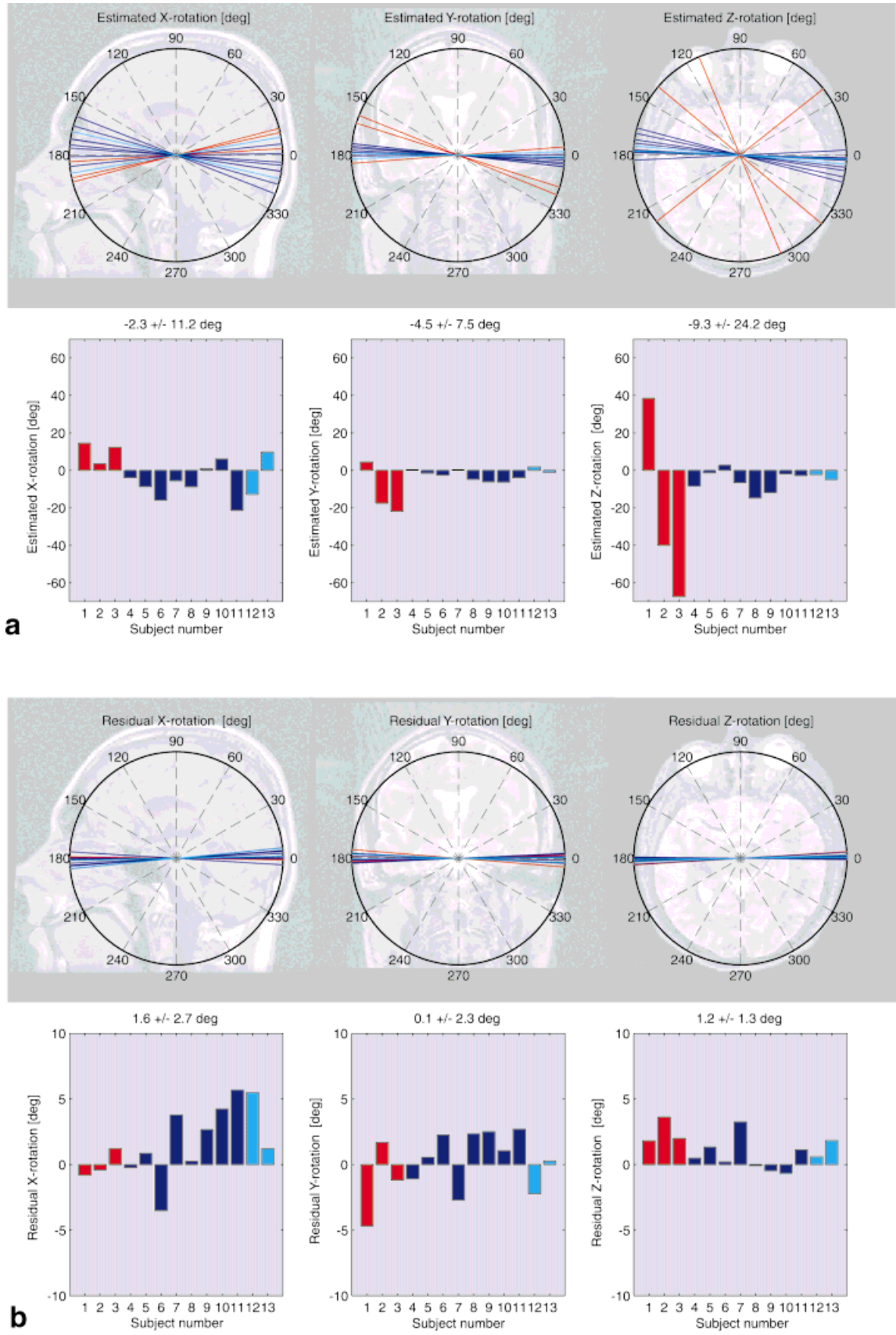

FIG. 4. Estimated (**a**) and residual (**b**) rotation angles for the 13 subjects in the training set (used to optimize the algorithm). In red are shown the three subjects who had been intentionally placed in the scanner with large rotation angles relative to typical patient positioning. In cyan are shown the two subjects who had large amounts of water in their nasal sinuses (due to sinusitis); their sinuses were incorrectly included in the brain surface by the automatic segmentation algorithm. The residual rotation angles of these five subjects fall within the range of the other subjects (dark blue).

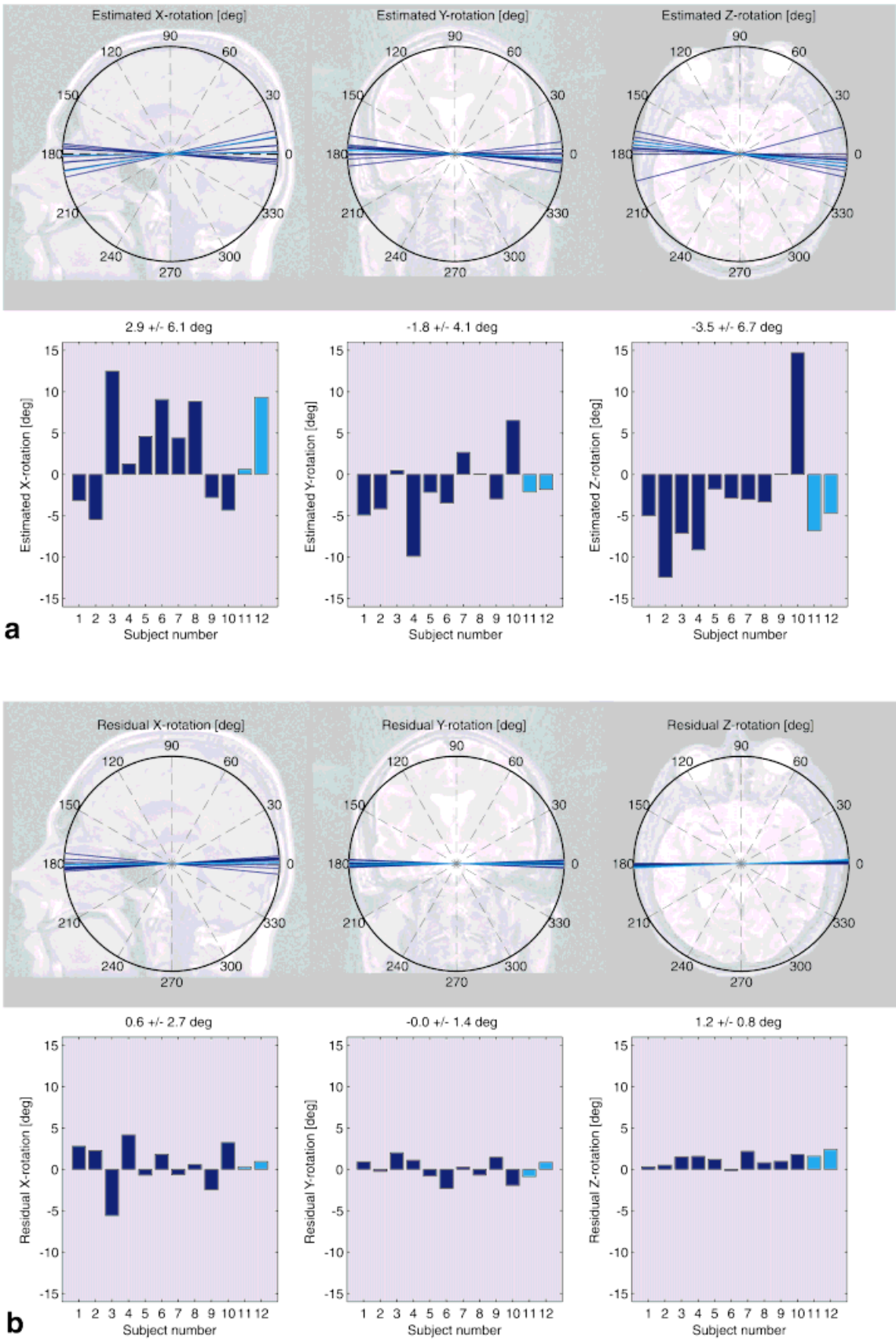

FIG. 5. Estimated (**a**) and residual (**b**) rotation angles for the 12 subjects in the test set processed without further modifications after optimizing the algorithm on the training set. The algorithm yields robust results for all 12 subjects, including two who had large amounts of water in their nasal sinuses (cyan). The ranges of residual rotation angles are similar to those obtained with the training set (Fig. 4).

Table 1
Estimated Rotation Angles, Residual Rotation Angles, and Residual Surface Matching Distance

Subject	Estimated			Residual			Distance (mm)
	X-rotation (deg)	Y-rotation (deg)	Z-rotation (deg)	X-rotation (deg)	Y-rotation (deg)	Z-rotation (deg)	
Training set							
1	14.56	4.47	38.51	−0.81	−4.68	1.82	2.54
2	3.54	−17.49	−40.01	−0.40	1.69	3.63	3.25
3	12.33	−21.89	−67.40	1.22	−1.19	2.00	3.41
4	−3.84	0.33	−8.39	−0.24	−1.07	0.50	3.17
5	−8.70	−1.54	−1.38	0.88	0.55	1.35	2.91
6	−15.92	−2.61	2.71	−3.51	2.26	0.22	3.67
7	−5.52	0.31	−6.57	3.78	−2.70	3.26	2.55
8	−8.80	−4.79	−14.77	0.25	2.34	−0.08	3.08
9	0.86	−6.14	−11.84	2.68	2.51	−0.47	2.55
10	6.07	−6.23	−1.96	4.23	1.07	−0.67	3.03
11	−21.33	−3.98	−2.79	5.67	2.70	1.15	3.11
12	−12.80	1.90	−2.28	5.49	−2.22	0.60	3.20
13	9.78	−1.06	−4.97	1.22	0.27	1.84	3.05
Average	**−2.29**	**−4.52**	**−9.32**	**1.57**	**0.12**	**1.16**	**3.04**
SD	11.23	7.47	24.19	2.68	2.33	1.33	0.34
Test set							
1	−3.16	−4.92	−5.02	2.81	0.93	0.32	2.76
2	−5.44	−4.18	−12.45	2.26	−0.24	0.52	2.71
3	12.49	0.48	−7.13	−5.58	2.00	1.53	2.90
4	1.26	−9.90	−9.14	4.17	1.11	1.58	2.93
5	4.62	−2.17	−1.76	−0.71	−0.82	1.21	2.83
6	9.07	−3.46	−2.86	1.85	−2.30	−0.15	3.02
7	4.41	2.68	−3.05	−0.66	0.26	2.20	3.09
8	8.84	0.03	−3.34	0.59	−0.70	0.83	3.63
9	−2.81	−2.96	0.04	−2.48	1.47	0.99	2.19
10	−4.32	6.54	14.71	3.26	−1.96	1.79	2.78
11	0.62	−2.13	−6.81	0.29	−0.87	1.60	3.21
12	9.34	−1.80	−4.70	0.94	0.87	2.38	3.68
Average	**2.91**	**−1.82**	**−3.46**	**0.56**	**−0.02**	**1.23**	**2.98**
SD	6.11	4.08	6.66	2.70	1.35	0.76	0.40

SD, standard deviation.

sets, respectively. As mentioned previously, the initial angles for the first three subjects are particularly large because these subjects had been intentionally placed in the scanner with severely tilted head orientations (Fig. 2). Four subjects had large amounts of water in their nasal sinuses, which were included in the brain surface by the surface segmentation algorithm. For these subjects, the second surface matching step, with the refined distance map, allowed the algorithm to ignore the sinuses and accurately recover scan orientations. For all other subjects, this second matching had no effect.

After matching, the average generalized distance between the patient and template brain surfaces was 3.04±0.34 mm (training set) and 2.98±0.40 mm (test set; Table 1). The residual rotation angles between template and reoriented pilot scans according to the geometric transformation derived by the algorithm are shown in Table 1. Note that the subjects with either large initial rotations (subjects 1–3 of training set), or water in the nasal sinuses (subjects 12 and 13 of the training set, and subjects 11 and 12 of the test set), do not appear as outliers in the results, but yield residual rotation angles within the range obtained for the other subjects. This suggests that the surface matching algorithm was robust with respect to initial conditions and to possible artifacts on the brain surface in the region of the nasal sinuses. The average 3D distance between landmarks was reduced by our algorithm from 40.5 ± 25.0 mm to 6.9 ± 2.9 mm for the training set, and from 35.8 ± 9.7 mm to 6.2 ± 2.0 mm for the test set. The scaling parameters recovered by our algorithm were 0.999 ± 0.026 for the training set (average of values for x, y, and z) and 0.998 ± 0.029 for the test set, indicating very small differences in brain size between subjects and template.

As an example of the quality of our algorithm, Fig. 2a shows MR images from one of the three volunteers with severely tilted head orientation (see also Table 1 and Fig. 4, subject 3 of training set). The matching algorithm recovered rotations of 12°, 22°, and 67° (x, y, and z) relative to the template scan. A repeat scan, acquired with the scanning geometry derived from the automatic prescription algorithm, showed symmetric brain structures (Fig. 2b) and closely resembled the template scan (Fig. 2c).

DISCUSSION

This study demonstrates the feasibility of automatic prescription of scan planes for brain MRI. The total time for

the autoprescription, including pilot scan and image processing, was approximately 30 sec, which is short enough for an automated prescan protocol. The use of single-shot FSE images, showing CSF only, allowed efficient extraction of the brain surface of the current subject with no user interaction. The surface matching algorithm proved very robust with respect to initial positioning and to surface segmentation artifacts. Our algorithm also provides a quality control measure, the generalized distance (in mm) between the current and the template brain surfaces. This measure could be used to initiate a manual procedure if it is found to be above a certain threshold, indicating a failure of the surface matching.

The emphasis of the present study is to develop a rapid and robust algorithm with reasonable accuracy. The relatively low residual rotation angles consistently measured for all subjects are within the expected error margin of a human operator who uses interactive graphical prescription tools. These residual angles might be further reduced at the cost of increased computational expense. For example, using the pilot scans at full resolution may yield slightly more accurate surface segmentation. However, since the two brain surfaces to be matched are from different subjects, interindividual differences in the brain shape may limit the potential gain in accuracy with increased spatial resolution. If the lower resolution is used in a routine implementation, scans should be acquired at reduced resolution, rather than at a high resolution followed by down-sampling.

Two special measures markedly improved the robustness of our algorithm. First, the eyes were automatically detected, and subsequently eliminated from the brain segmentation. Second, exclusion of the nasal sinuses in the second surface matching step significantly improved the matching in subjects with large amounts of water in the sinuses. In the subjects in whom the surface segmentation algorithm correctly excluded the nasal sinuses, the second matching step yielded transformation parameters identical to those from the first matching step. Because the alternate distance map (sinuses excluded) is spatially less complete than the original one, correct matching in the second matching step relies on a fairly accurate adjustment of the current brain surface to the template surface by the first matching step. Therefore, the use of two successive surface matching steps is more robust than a single-step matching algorithm that uses only the alternate distance map.

Our sample datasets included male and female subjects, both normal controls and patients, and sampled a range of possible head positions and orientations. We have previously studied the effect on our surface matching algorithm of artificially introducing a large structural defect (an ellipsoid with diameters of $10 \times 20 \times 40$ mm was cut out of the frontal lobe of one of two surfaces to be coregistered). For 11 coregistrations, we found that this artificial artifact only slightly degraded registration accuracy, by about 0.5° in x, y, and z rotation, and 0.25 mm in x, y, and z translation (3). Together with the good surface matching results reported in the present study when surface segmentation artifacts were encountered (in the region of the nasal sinuses), these findings suggest that our algorithm is robust to structural differences between the current and template brain surfaces. Furthermore, our method for overcoming surface segmentation artifacts in the nasal sinuses could be generalized to other regions of the head if future studies demonstrate frequent segmentation or registration problems for particular patient populations.

One of the consequences of the limited use of the available freedom in scanning geometry in manual prescription by human operators is a nonstandardized prescription, which yields scan orientations that vary from one patient to another. This intersubject variability can make interpretation of the images more difficult, and may ultimately lead to reduced quality of radiologic readings. Another consequence of the variability in the scan orientations is limited intrasubject reproducibility for repeat scans. Very different images may be obtained when the same subject is scanned in different sessions, such as for follow-up medical evaluations, making direct comparison of scans from different sessions unnecessarily difficult. Although a *posteriori* coregistration and realignment of follow-up scans have been demonstrated in research studies, these techniques have not yet been integrated into the standard clinical environment. Most diagnostic interpretation is performed on films or electronic displays of the scans in their native orientation, especially since post hoc reorientation may yield image degradation when the image resolution is not isotropic. In contrast, our method could be used in routine clinical settings since it corrects for patient positioning prior to scan acquisition and requires no human interaction. Furthermore, although we have included only a geometric description of scanning volume boundaries in our template, future implementations of our technique could include other geometric objects, such as locations of MR spectroscopy voxels, or a narrow range of slice positions for detailed imaging of anatomical structures such as the pituitary gland.

Our matching algorithm currently determines the translation, scaling, and rotation parameters between the reference and the new brains. Additional parameters, such as shearing, could also be determined by the same algorithm by allowing all nine parameters in the transformation matrix A (Eq. [1]) to be optimized (9). While this may improve the quality of the surface matching algorithm, it poses the problem of recovering pure rotation angles from the transformation matrix determined by the algorithm.

In summary, automatic scan prescription promises many future improvements over manual prescription, including reduced scan times, reproducible intersubject scan orientations along anatomically preferable orientations (such as the anterior-commissure posterior-commissure (AC-PC) line), and better reproducibility for intrasubject repeat studies. Our study demonstrates the feasibility of automatic scan prescription for the brain with high accuracy.

ACKNOWLEDGMENT

U.S. Patent (#09/272, 436).

REFERENCES

1. Van den Elsen PA, Pol ED, Viergever MA. Medical image matching—a review with classification. IEEE Eng Med Biol 1993;12:26–39.

2. Pelizzari C, Chen G, Spelbring D, Weichselbaum R, Chen C. Accurate three-dimensional registration of CT, PET, and/or MR images of the brain. J Comput Assist Tomogr 1989;13:20–26.
3. Itti L, Chang L, Mangin JF, Darcourt J, Ernst T. Robust multimodality registration for brain mapping. Hum Brain Map 1997;5:3–17.
4. Ende G, Treuer H, Boesecke R. Optimization and evaluation of landmark-based image correlation. Phys Med Biol 1991;37:261–271.
5. Wang C, Pahl JJ, Hogue RE. A method for co-registering three-dimensional multimodality brain images. Comput Methods Prog Biomed 1994;44:131–140.
6. Woods R, Mazziotta J, Cherry S. MRI-PET registration with automated algorithm. J Comput Assist Tomogr 1993;17:536–546.
7. Friston KJ, Ashburner J, Poline JB, Frith CD, Frackowiak RSJ. Spatial realignment and normalization of images. Hum Brain Map 1995;2:165–189.
8. Itti L, Chang L, Ernst T, Mishkin F. Improved 3-D correction for partial volume effects in brain SPECT. Hum Brain Map 1997;5:379–388.
9. Ernst T, Speck O, Itti L, Chang L. Simultaneous correction for interscan patient motion and geometric distortions in echo planar imaging. Magn Reson Med 1999;42:201–205.
10. Alpert NM, Berdichevsky D, Levin Z, Morris ED, Fishman AJ. Improved methods for image registration. Neuroimage 1996;3:10–18.
11. Mangin JF, Frouin V, Bloch I, Bendriem B, Lopez-Krahe J. Fast nonsupervised 3D registration of PET and MRI images of the brain. J Cereb Blood Flow Metab 1994;14:749–762.
12. Wacken PFM. Chamfer metrics in mathematic morphology. J Math Imaging Vision 1994;4:233–253.
13. Borgefors G. Distance transformations in digital images. Comp Vision Graph Image Proc 1986;34:344–348.
14. Powell MJD. An efficient method for finding the minimum of a function of several variables without calculating derivatives. Comput J 1964;7:155–163.